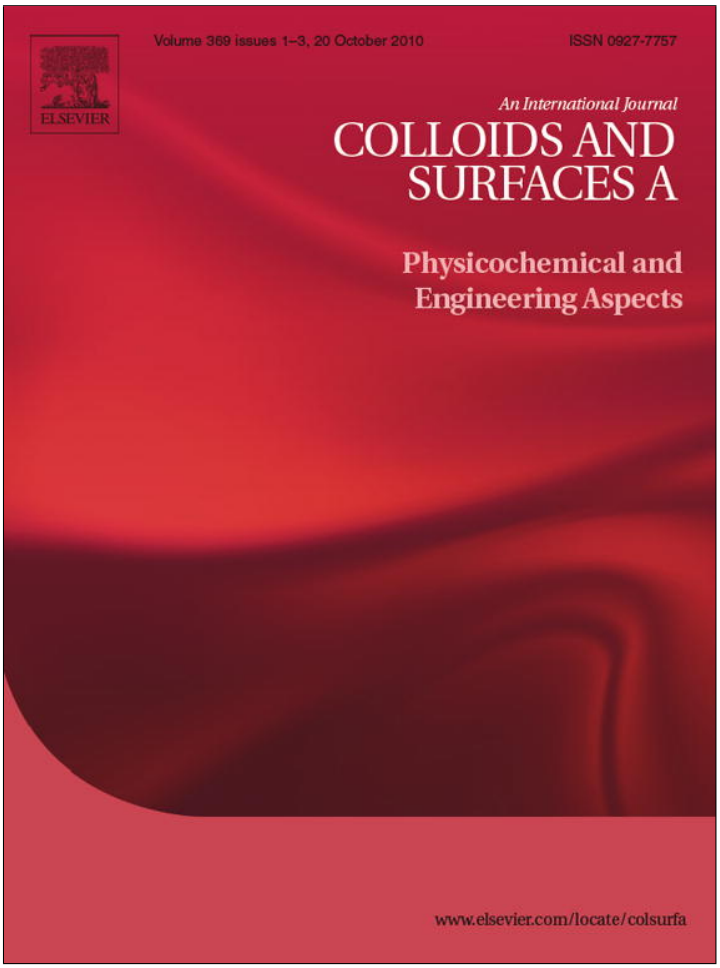

Colloids and Surfaces A: Physicochem. Eng. Aspects 369 (2010) 141–147

Contents lists available at ScienceDirect

Colloids and Surfaces A: Physicochemical and Engineering Aspects

journal homepage: www.elsevier.com/locate/colsurfa

Dynamics of dewetting

E. Bertrand, T.D. Blake*, J. De Coninck

Laboratory of Surface and Interfacial Physics (LPSI), University of Mons, 7000 Mons, Belgium

ARTICLE INFO

Article history:
Received 22 June 2010
Received in revised form 31 July 2010
Accepted 4 August 2010
Available online 11 August 2010

Keywords:
Wetting
Dewetting
Liquid entrainment
Sliding drops
Contact-line friction
Coating

ABSTRACT

The dynamics of dewetting is re-examined from a theoretical perspective and in the light of experiment. Two cases are considered: (a) spontaneous dewetting following rupture of a thin liquid film previously formed on a partially wetted solid surface; (b) steady dewetting when a partially wetted solid surface is withdrawn vertically from a pool of liquid. In the first, a rim of liquid forms at a circular dewetting front that expands at constant speed, while the remainder of the film remains quiescent. The second is characterised by the formation of a serrated contact line, in which each straight-line section also recedes at a constant normal velocity, but with no significant rim. These two cases are analysed in terms of the relevant dissipation processes. Hydrodynamic dissipation is estimated using a simple model proposed by de Gennes, while the molecular-kinetic theory accounts for contact-line friction. The new analysis suggests that for a given system, the dewetting velocities and dynamic contact angles seen in the two cases are likely to be different. In (a), they will be the outcome of both dissipation channels operating in parallel, whereas in (b), both parameters will be determined by a dynamic balance between the two sources of dissipation that avoids an inflection in the liquid–vapour interface near the receding contact line. These predictions are consistent with current observations and could be tested by well-designed experiments.

1. Introduction

The dewetting of a solid by a liquid is a commonplace phenomenon, important for a host of practical applications, from mineral flotation, oil recovery, detergency, lithography, and textiles to lubrication, microfluidics and self-cleaning windows. It also plays a role in many natural processes. The topic has been the subject of research over several decades and is increasingly well described. However, there remain significant gaps in our understanding and in our ability to model dewetting in sufficient detail to predict reliably key outcomes, such as the speed at which a given liquid can be made to dewet a given solid.

Here, we revisit the problem, making use of existing models to describe the dynamics of dewetting in simple terms, but with a new emphasis and a revised framework in which we stress the potential importance of contact-line dissipation. The models used are highly simplified and have well-known limitations. Nevertheless, they capture much of the underlying physics. Two cases are considered that are usually discussed in isolation, as if unrelated: (a) spontaneous dewetting following the rupture of a thin liquid film previously formed on a partially wetted solid surface; (b) steady dewetting when a partially wetted solid surface is withdrawn vertically from a pool of liquid. Dewetting proceeds differently in the two geometries, and this affects the way in which the models need to be applied to describe observed behaviour.

2. Dewetting following rupture of a thin film

Experimental studies of dewetting have paid particular attention to the rupture and dewetting of thin, metastable liquid films previously applied to partially wetted surfaces [1,2]. For simple liquids (excluding long-chain polymers), experiment has shown that, following either spontaneous or artificially initiated rupture, a nominally dry, circular hole, of radius R, develops and grows at a constant radial speed $U = dR/dt$, i.e. $R \propto t$. A characteristic and rather special feature of this type of dewetting is that the liquid from the film collects within a narrow rim or bead at the edge of the expanding hole. This bead exhibits a constant receding dynamic contact angle θ_D. Moreover, all the flow is within the bead and the capillary wave at its leading edge, while the remainder of the film is undisturbed. Similar results have been obtained in molecular-dynamics simulations [3,4]. The entire process is driven by the surface free energy released by the creation of new solid–vapour (SV) interface and the simultaneous loss of equal areas of liquid–vapour (LV) and solid–liquid (SL) interface, i.e.:

$$-\gamma_{SV} + \gamma_{LV} + \gamma_{SL} = \gamma_{LV}(1 - \cos\theta^0), \quad (1)$$

* Corresponding author. Tel.: +44 1442 824694.
E-mail address: terrydblake@btinternet.com (T.D. Blake).

0927-7757/$ – see front matter © 2010 Elsevier B.V. All rights reserved.
doi:10.1016/j.colsurfa.2010.08.006

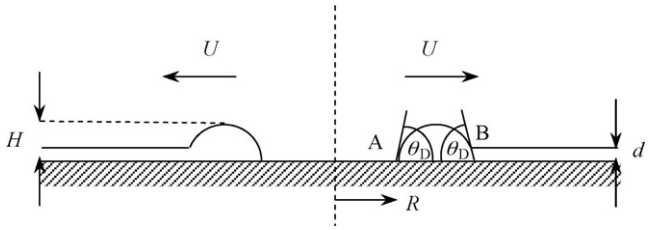

Fig. 1. Schematic cross-section through a liquid film dewetting a solid, showing the formation of the dry hole and the circular rim.

where γ_{SV}, γ_{LV} and γ_{SL} are the various interfacial tensions and, θ^0 is the equilibrium contact angle define by Young's equation:

$$\cos\theta^0 = \frac{\gamma_{SV} - \gamma_{SL}}{\gamma_{LV}}, \tag{2}$$

A complete solution of the hydrodynamic problem posed by the flow within the rim is challenging, as it involves both a free liquid surface and a moving contact line. Nevertheless, it has been shown that a reasonably good description can be obtained using a highly simplified model of the principal hydrodynamic channels by which the surface free energy is dissipated [1,5–7].

The general approach can be illustrated with reference to the idealised situation depicted in Fig. 1. Here, the cross-section of the rim is approximated by a circular arc. As the hole expands, the two main sources of dissipation are the flows near the receding three-phase contact line of the rim, A, and at the advancing capillary wave, B, which is treated as a pseudo contact line. The driving force available at the former is simply the out-of-balance surface tension force $F_A = \gamma_{LV}(\cos\theta_D - \cos\theta^0)$, and that at the latter is $F_B = \gamma_{LV}(1 - \cos\theta_D)$, where the apparent contact angle at B is assumed to be the same as that at A (the thickness of the film d is taken as negligible in comparison with the height of the rim H). $F_A + F_B$ is equal to the total driving force given by Eq. (1).

The hydrodynamic equations used to express U_A and U_B in terms of F_A and F_B are [1,5–7]:

$$U_A = \frac{\gamma_{LV}(\cos\theta_D - \cos\theta^0)\theta_D}{3\eta_L \ln l_A} \approx \frac{\gamma_{LV}((\theta^0)^2 - (\theta_D)^2)\theta_D}{6\eta_L \ln l_A} \tag{3}$$

$$U_B = \frac{\gamma_{LV}(1 - \cos\theta_D)\theta_D}{3\eta_L \ln l_B} \approx \frac{\gamma_{LV}(\theta_D)^3}{6\eta_L \ln l_B} \tag{4}$$

where η_L is the shear viscosity of the liquid and l_A and l_B the ratios of appropriately chosen macroscopic and microscopic length scales. These expressions are based on a simple lubrication model in which the variation of the contact angle is determined by viscous dissipation at the mesoscopic scale [5].

For a rim to persist the velocities of points A and B must be approximately the same, i.e. $U_A \approx U_B$ and the rim grows only slowly [6]. Equating Eqs. (3) and (4) and assuming $l_A \approx l_B = l$, yields:

$$\theta_D \approx \frac{\theta^0}{\sqrt{2}}. \tag{5}$$

Inserting this value in either Eq. (3) or (4) gives the final result that:

$$U_A \approx U_B \approx U^*(\theta^0)^3, \tag{6}$$

where $U^* = \gamma_{LV}/12\sqrt{2}\eta_L \ln l$ is constant for a given system. This simple relationship has been shown to hold remarkably well by Redon et al. [1] in elegant experiments with silicone oils and alkanes on silicon wafers grafted with fluorinated or aliphatic silicones. Furthermore, the ratio θ_D/θ^0 was found to be 0.7 ± 0.2, which is close to the predicted value.

The experimental confirmation of the cubic law has tended to be interpreted as evidence that all aspects of dewetting are described by simple hydrodynamics. However, one aspect of the problem seems to have been overlooked, specifically the possibility that dissipation mechanisms other than simple viscous flow might be important at the receding contact-line A. The fact that a rim persists, i.e. $U_A \approx U_B = U$, means that zones A and B are coupled by the flow and that the energy dissipation at both is approximately the same, i.e. $\sim -USc^0/2$. In the model outlined above, the assumption of a common dynamic angle at A and B ensures that the dissipation is precisely the same. Note also that at A, θ_D is a receding angle which decreases with increasing U_A, whereas, at B, θ_D is an advancing angle which increases with U_B. Any change in U would therefore cause the angles at A and B to diverge. Collectively, these arguments show that both zones are important in regulating the growth of the hole.

Let us therefore consider this situation in more detail. While there is no reason to doubt that the rate of advance of B (which is, in any case, a capillary wave and not a contact line) is controlled by hydrodynamics, there are good reasons for considering alternative mechanisms for dissipation at the true contact-line A.[1] These stem from the problem of reconciling a contact line that moves with the standard no-slip boundary condition at the SL interface [11–15]. This problem has been the source of much debate for at least the last 40 years, but the details need not concern us here. It is sufficient to recognise that the observation of an apparently cubic law for the growth of the hole in the film does not preclude the possibility that the dynamics at A is controlled by channels of dissipation in addition to those of bulk viscous flow. We therefore need to consider alternative models for this region to see if they also agree with experiment and could improve our understanding.

One such model is that proposed by Shikhmurzaev [14,16], which accommodates dissipation through standard hydrodynamic channels (Stokes flow), but also exploits non-equilibrium thermodynamics to describe dissipation due to the interfacial changes occurring as the contact-line moves across the solid surface. It would be interesting to see this model applied specifically to dewetting, either in a full numerical analysis or in its asymptotic form. The model could be augmented by experiment and simulation to determine the key interfacial properties required by the model. Although potentially the most self-consistent, such an approach is well beyond the scope of the present paper. Here we employ the much simpler model of contact-line dynamics known as the molecular-kinetic theory (MKT) [17,18]. This model successfully rationalizes the dynamic wetting behaviour seen with a wide range of experimental systems [15,18]. It is also effective in accounting for dewetting dynamics in simple systems, such as when a small bubble or drop is pressed against a hydrophobic plate under water [19,20], a geometry of particular relevance to mineral flotation. Moreover, recent molecular-dynamics simulations have shown the model to have validity at the microscopic scale [21–23]. The model is described at length elsewhere, but it is helpful to recapitulate the main assumptions and equations.

According to the MKT, the motion of the contact line is determined by the statistical dynamics of the fluid molecules within the three-phase zone (TPZ) where the solid, liquid and gas phases meet [17,18]. On the molecular scale, this zone has a finite size, which is comparable to the thickness of its confluent interfaces, but is otherwise unspecified. The approach is based on the Frenkel–Eyring treatment of fluid transport as a stress-modified molecular rate process. The key parameters are κ^0, the equilibrium frequency of the thermal displacements of liquid molecules at the SL interface

[1] For <fn0005>polymer films, there is evidence of significant slip between the polymer and the solid. This provides an additional channel of dissipation and may substantially modify both the shape of the rim and the rate of expansion of the hole [2,8–10]. Such considerations can probably be ignored for simple liquids, except perhaps for very thin films on the most poorly wetted substrates.

within the TPZ and λ the average distance of each displacement.

The MKT is based on the idea that the velocity-dependence of the dynamic contact angle is due to the disturbance of adsorption equilibria at the various interfaces and, hence, to changes in the local surface tensions as the contact-line moves across the solid surface and SL interface is created or destroyed. These changes in surface tension lead directly to the driving force for dewetting $F_A = \gamma_{LV}(\cos\theta_D - \cos\theta^0)$. It is worth noting that the Shikhmurzaev model contains the same underlying concept, absent from earlier hydrodynamic treatments, which usually assume that the local, microscopic angle is unaltered from its equilibrium value [12,13]. In the MKT, F_A is dissipated irreversibly within the TPZ in overcoming energy barriers to molecular displacements across the solid surface. The energy barriers may arise from many sources, including simple adsorption and pinning at nano-scale roughness and heterogeneity, and, provided they are susceptible to Maxwell–Boltzmann statistics, may all contribute to the observed kinetics, though possibly over different timescales [18]. The final equation for the velocity of dewetting is:

$$U = 2\kappa^0\lambda \sinh \frac{[\gamma_{LV}(\cos\theta_D - \cos\theta^0)]}{2nk_BT}, \quad (8)$$

where n is the number of adsorption sites per unit area, k_B is the Boltzmann constant and T the absolute temperature.

The characteristic frequency κ^0 may be written in terms of the activation free energy of wetting ΔG^*_w as:

$$\kappa^0 = \left(\frac{k_BT}{h}\right) \exp\left(\frac{-\Delta G^*_w}{N_A k_B T}\right), \quad (9)$$

where h and N_A are the Planck constant and Avogadro number, respectively. If the adsorption sites are distributed uniformly and molecules move only between adjacent sites, then $n \sim 1/\lambda^2$. In this case Eq. (8) contains only two unknown parameters, κ and λ, whose values can be obtained by fitting the equation to experimental data. While λ is usually of molecular dimensions, κ^0 can vary widely, and generally decreases with increasing viscosity and SL interaction [15,18].

If the argument of the sinh function in Eq. (8) is small, e.g. if the system is not too far from equilibrium, then the equation reduces to the linear form:

$$U = \frac{\gamma_{LV}}{\zeta}(\cos\theta_D - \cos\theta^0), \quad (10)$$

where $\zeta = nk_BT/\kappa^0\lambda \approx k_BT/\kappa^0\lambda^3$ is the coefficient of contact-line friction [21]. This coefficient has the same units as viscosity; thus Eq. (10) can be rearranged to give:

$$\cos\theta_D = \cos\theta^0 + Ca_{CL} \quad (11)$$

where $Ca_{CL} = U_A\zeta/\gamma_{LV}$ defines a capillary number based on contact-line friction.

It has recently been shown [22–26] that contact-line friction is proportional to the viscosity of the liquid, but exponentially dependent on the work of adhesion between the liquid and the solid $Wa^0 = \gamma_{LV}(1 + \cos\theta^0)$:

$$\zeta \approx \frac{\eta_L v_L}{\lambda^3} \exp\left(\frac{Wa^0}{nk_BT}\right), \quad (12)$$

where v_L is the molecular flow volume of the liquid and Wa^0 approximates the specific activation free energy of wetting due to SL interactions. Thus, the equilibrium wettability of the substrate can have a profound influence on wetting dynamics.

Several authors have combined the MKT with hydrodynamic theory to give a composite model that accommodates both contact-line friction and viscous dissipation channels [6,27–29]. That due to de Gennes [5] may be written for dewetting as:

$$U = \frac{\gamma_{LV}(\cos\theta_D - \cos\theta^0)}{\zeta + 3\eta_L/\theta_D \ln l_A}. \quad (13)$$

Here, Eqs. (3) and (10) have been combined by simply adding the dissipation due to contact-line friction, $U\zeta$, to that due to flow, $U(3\eta_L \ln l_A/\theta_D)$. The presence of the contact angle in the denominator makes the viscous term the controlling influence at sufficiently small angles.

We are now in a position to explore the consequences of combining Eqs. (8), (10) or (13) with (4) to describe the dynamics of dewetting with a rim and compare it with Eqs. (5) and (6). The simplest combination that captures the essence of our argument is to use Eq. (10) at A and Eq. (4) at B. Setting $U_A \approx U_B$, as before, we find:

$$\theta^0 \approx [c_B(\theta_D)^3 + (\theta_D)^2]^{0.5}, \quad (14)$$

where $c_B = \zeta/3\eta_L \ln l_B$. Estimates of ζ based on published dynamic contact angle data for silicone oils suggest ζ/η_L is about 40 [15]. Estimates of the logarithmic term l_B range from 9 to 20 [1]; hence, c_B is probably of order 1 for such systems. Using this value, we have evaluated Eq. (14). The results are plotted in Fig. 2 and compared with the prediction of Eq. (5): $\theta_D/\theta^0 \approx 1/\sqrt{2}$.

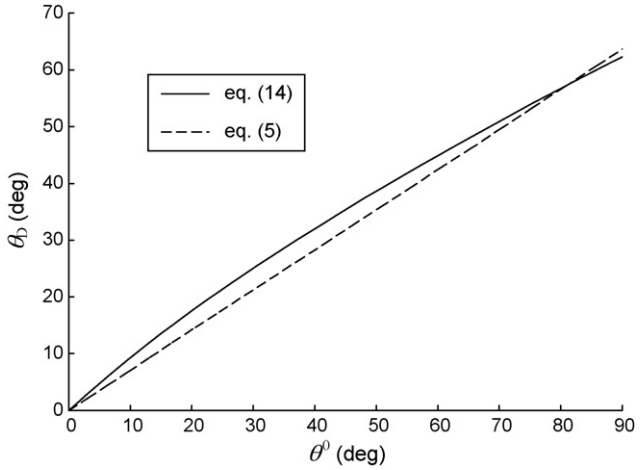

Fig. 2. Comparison of the predictions of the contact-line friction (Eq. (14)) and hydrodynamic models (Eq. (5)).

From this it is clear that over the range of equilibrium contact angles investigated by Redon et al. (15–60°) the predictions of the hydrodynamic and the contact-line friction models are indistinguishable within the experimental uncertainty (0.7 ± 0.2). Values of c_B from about 0.5 to 5 also give lines that lie within this range and should therefore give rise to a relationship between U and θ^0 not easily distinguished from the cubic law predicted by Eq. (6). Very recent molecular-dynamics studies by Bertrand [30] support this conclusion. It would therefore be of interest to explore this problem experimentally for systems having a broad range of ζ/η_L values.

Much the same result can be obtained using Eq. (8) or (13). Evidently, it is hard to judge which model is the most effective without more information; in particular, accurate data on the dynamic contact angle as a function of contact-line velocity would be highly desirable, since these would enable us to determine a value for ζ.

3. Dewetting of a draining film

We now turn to a second type of dewetting in which a thin film of liquid drains under gravity from a partially wetted solid surface [27,31–34]. Consider such a surface withdrawn vertically from a pool of liquid at velocity U. As the rate of withdrawal is increased,

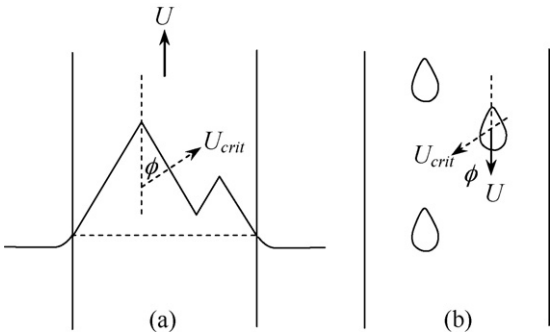

Fig. 3. (a) Formation of a serrated contact line as a partially wetted tape is withdrawn from a pool of liquid. (b) Drops running down a partially wetted surface.

θ_D falls steadily until, at some critical velocity U_{crit}, liquid begins to be entrained by the moving solid, i.e. the liquid coats the solid. If the solid is rectilinear, e.g. a tape or sheet (Fig. 3a), this dynamic wetting transition is characterised by the formation of a serrated contact line, each straight-line section of which is slanted at an angle ϕ to the direction of withdrawal, such that the velocity of the receding contact line normal to itself remains constant [33]:

$$U_{crit} = U \cos \phi. \quad (15)$$

In this type of dewetting, no significant bead is formed below the receding contact line[2] and the whole film drains under gravity. As a result, the rate of dewetting is controlled entirely by the dynamics of the contact line and we therefore need to consider dissipation in this region only. Since the same surface tension driving force is available, then, all else being equal, one might anticipate a higher dewetting speed and hence a smaller dynamic contact angle than when a rim is present. At sufficiently high speeds $U_{drop} > U_{crit}$, liquid rivulets are entrained from trailing vertices, which break into droplets due to Raleigh–Taylor instability [33].

There are strong similarities between dewetting during drainage and a liquid drop running down a partially wetted surface (Fig. 3b), such as a raindrop moving down a windowpane [35–37]. At sufficiently high speeds, these drops also exhibit a trailing vertex. It should be noted, however, that gravitational drainage is not a prerequisite for the occurrence of serrated contact lines. They also characterise the onset of air entrainment in liquid coating processes, irrespective of substrate width and orientation [38], and are seen during wettability-directed dewetting in patch coating [39]. Thus, it would seem that provided the geometry of the system is favourable, serrated contact lines are the norm once critical wetting or dewetting speeds are exceeded.

It was initially thought that the dynamic receding contact angle θ_{crit} at U_{crit} was close to zero [31–33], but this is not the general case. As U is increased and θ_D decreases, the viscous stress within the narrowing wedge of liquid will grow and must eventually exceed the opposing surface tension stress at some non-zero meniscus slope angle, leading to a dynamic wetting transition at some critical capillary number $Ca_{crit} = \eta_L U_{crit}/\gamma_{LV}$. The question then arises as to what precisely determines U_{crit} for any given system. In particular, is the limit affected by sources of dissipation other than simple viscous flow?

One of the characteristics of a dynamic wetting transition (i.e. a transition between steady dewetting and liquid entrainment, sometimes known as a Landau–Levitch transition) is the appearance of a visible inflection in the liquid meniscus [27,40]. Together

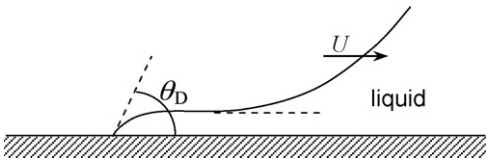

Fig. 4. Inflection in the liquid–vapour meniscus at or near a dynamic wetting transition, giving an apparent dynamic receding contact angle of zero.

with hydrodynamic arguments, this has lead some authors to conclude that even if the inner, microscopic contact angle at U_{crit} is not zero, the apparent contact angle made by extrapolating the outer liquid meniscus is indeed zero (Fig. 4), and to use this criterion to estimate U_{crit} [40–42]. If this were always the case, we might expect the entrained film to grow indefinitely and coat the solid surface once the critical velocity had been exceeded. There would then be complete separation of the main flow from the contact line, which would recede more slowly at $U < U_{crit}$ with a contact angle $\theta_D > \theta_{crit}$. Such divergent behaviour, does seem to occur in some geometries, such as when a liquid is displaced sufficiently rapidly from a capillary tube (radii of the order of millimetres) [43,44] or a fibre or cylindrical rod (radii from millimetres to centimetres) is pulled from a bath of liquid [40,45,46]. However, in such cases, there are no edges to initiate a serrated contact line, and instabilities have been reported leading to the formation of droplets [45], which suggests an underlying tendency to revert to the serrated pattern. Furthermore, at sufficiently high speeds, running drops always seem to exhibit the familiar teardrop shape with a single trailing apex unless they leave a wetting film.

de Gennes [5] has pointed out that Eq. (3) has a maximum at $\theta_D \approx \theta^0/\sqrt{3}$, yielding $U_{crit} \approx \gamma_{LV}(\theta^0)^3/9\sqrt{3}\eta_L \ln l_A$, beyond which, the contact line should vanish; thus providing a possible rationale for the dynamic wetting transition. An alternative explanation [42,47] is based on the issue of matching the interfacial curvature of the inner region near the contact line to that of the outer meniscus once the capillary number exceeds some critical value. This analysis uses the Voinov–Cox hydrodynamic model of dynamic wetting [12,13], and assumes the microscopic angle to be fixed and equal to θ^0. Of particular interest here, however, is the acknowledgement that if there are other sources of dissipation at the contact line in addition to viscous dissipation in the bulk of the liquid, the microscopic contact angle will be forced towards smaller values, leading to a reduction in U_{crit} [42]. Unfortunately, this possibility does not seem to have been explored. Nevertheless, it may be indicative that Eq. (13) for the combined hydrodynamic-molecular-kinetic model exhibits a maximum at a dynamic angle that depends on ratio of contact-line friction to viscosity. In this case, the maximum occurs at:

$$\theta^0 = \theta_D \left(\frac{2\zeta\theta_D}{3\eta_L \ln l_A} + 3 \right)^{0.5}. \quad (16)$$

This gives de Gennes's prediction when ζ is small, but implies that $\theta_{crit} \to 0$ as ζ/η_L becomes large. Fig. 5 illustrates the trend for increasing levels of contact-line friction with $\ln l_A^* = 10$, $\theta^0 = 80°$ and $\eta_L = 23$ mPa s, which are the same values as used for Fig. 7, below, to allow comparison.

On the other hand, the formation of a serrated contact line does not seem consistent with a sudden divergence from steady wetting to complete entrainment. The way in which the inclination angle ϕ continuously adjusts to maintain a constant contact-line velocity implies a steady state, with a dynamic balance between surface tension and viscous forces. We therefore suggest that such a balance might be achieved when the meniscus slope angle resulting from the hydrodynamic dissipation equals the contact angle resulting from a local dissipation mechanism such as contact-line friction.

[2] Snoeijer <fn0010>et al. [34] have reported an upward propagating capillary ridge or shock that was not detected previously [33]. It is not yet clear how ubiquitous this ridge is.

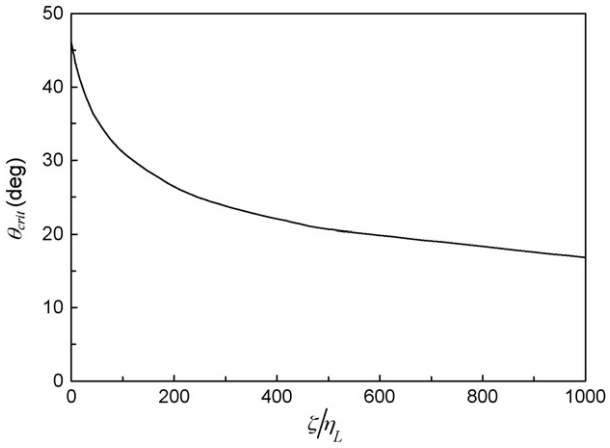

Fig. 5. Critical dynamic contact angle θ_{crit} as a function of the dimensionless ratio of contact-line friction to viscosity ζ/η_L. Curve calculated using Eq. (16) and the same values of η_L, γ_L, θ^0 and $\ln l_A^*$ as for Fig. 7.

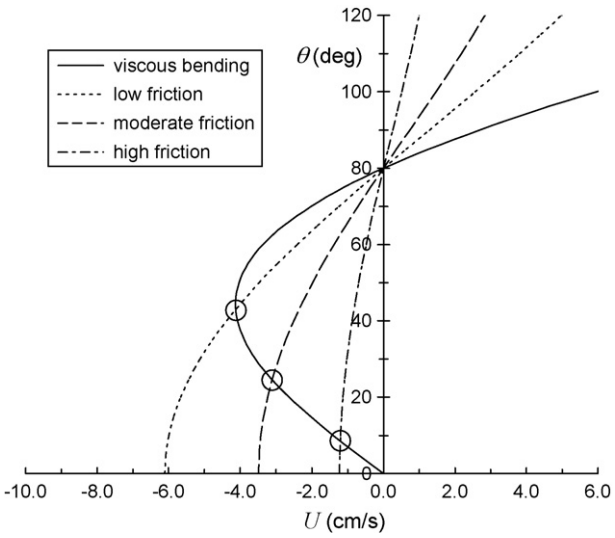

Fig. 7. Graphical solution of Eqs. (3) and (10) for increasing levels of contact-line friction for $\ln\ l_A^* = 10$, $\gamma_L = 68$ mN/m, $\theta^0 = 80^\circ$ and $\eta_L = 23$ mPa s. Dewetting velocities are shown here as negative values.

Since the change in the contact angle from its equilibrium value is a measure of the dissipation, this is equivalent to saying that the balance will be achieved when the rate of hydrodynamic dissipation in the liquid wedge equals that at the contact line. That the two sources of dissipation become comparable near θ_{crit} has previously been noted by Petrov [41]. So long as the meniscus slope remains greater than or equal to the local dynamic angle, an inflection will be avoided. Only if the meniscus slope and the local angle fall below some critical value will viscous dissipation become dominant, creating an inflection and triggering separation of the contact line from the bulk meniscus. This is illustrated in Fig. 6.

The energy incentive for a balance to be maintained comes from the surface free energy cost of generating additional non-equilibrium LV and SL interface at the expense of SV interface. Provided the contact line can orient in such a direction as to avoid this penalty, it will do so. Along the slanted sections, the balance will therefore be self-regulating at $U = U_{crit}$ with $\theta_D = \theta_{crit}$.

At a trailing vertex, this mechanism is not available and liquid will be entrained, but onset will be postponed to a higher velocity than U_{crit} by the steep curvature of the meniscus in this region. This creates a pressure gradient opposing that generated by the flow in the wedge, driving the flow towards the liquid and so increasing meniscus slope [47]. Since the dewetting velocity will be higher here than along the slanted sections of the contact line, the local contact angle should be smaller, something that could be checked experimentally. Nevertheless, at sufficiently high speeds, a rivulet will be entrained, which will break into drops—the so-called "pearling transition" [35]. The only detailed study of the dynamic contact angle in this region known to the authors is that of Rio, et al. [36], in which the dynamic contact angle was measured at various points around a sliding drop. This careful work confirms that the contact angle depends everywhere on the local velocity normal to the contact line.

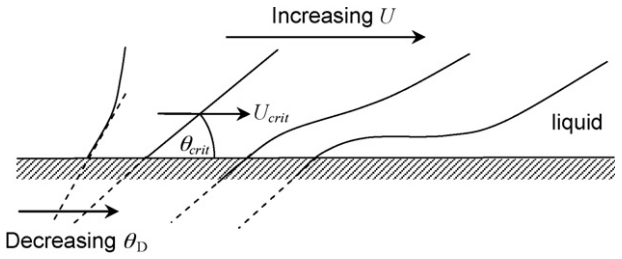

Fig. 6. Schematic illustration of a dynamic wetting transition on increasing the dewetting speed U. Complete entrainment is avoided if the contact line can align such that its normal velocity remains constant at U_{crit}.

Based on this idea of a balance between viscous and surface forces, it should be possible to make a rough estimate of θ_{crit} and U_{crit} by solving Eqs. (3) and (10) simultaneously.[3] The former provides an approximate expression for the slope angle of the LV interface due to viscous bending in the absence of contact-line friction, while the latter gives the angle due to contact-line friction in the absence of viscous bending. These equations have one trivial solution at $\theta_D = \theta^0$, $U = 0$, and another at:

$$\theta_D = \frac{1}{c_A}, \tag{17}$$

$$U = \frac{\gamma_{LV}}{\zeta}(\cos\theta_D - \cos\theta^0) \approx \frac{\gamma_{LV}}{2\zeta}((\theta^0)^2 - (\theta_D)^2), \tag{18}$$

where $c_A = \zeta/3\eta_L \ln l_A$. Here, we have used Eq. (10) to calculate U_D from θ_D. Eq. (17) can also be obtained simply by setting the frictional dissipation equal to that due to viscous flow: $\zeta U = 3\eta_L U \ln l_A/\theta_D$. This solution exists only if the dissipation due to contact-line friction initially exceeds that due to viscous bending as the dewetting velocity is increased from zero, i.e. $\zeta > 3\eta_L \ln l_A/\theta^0$. Under these conditions, the apparent contact angle will be determined by contact-line friction until the capillary number is sufficiently high for viscous dissipation to reduce the meniscus slope angle to a lower value. The higher the friction relative to viscosity, the smaller this angle will be. Interestingly, the angle given by Eq. (17) does not depend explicitly on θ^0. For solutions giving angles $\theta_D > \theta^0/\sqrt{3}$, behaviour will subsequently be described by Eq. (3) with θ_{crit} at $\theta^0/\sqrt{3}$ (assuming de Gennes's simplified model holds). However, for sufficiently high friction, the solution will give $\theta_D < \theta^0/\sqrt{3}$ and a dynamic balance will be necessary to avoid entrainment.

Graphical solutions to Eqs. (3) and (10) with these constraints are illustrated in Fig. 7 for increasing levels of contact-line friction ($\zeta = 40\eta_L$, $70\eta_L$ and $200\eta_L$), taking $\ln l_A^* = 10$ and using values of $\gamma_L = 68$ mN/m, $\theta^0 = 80^\circ$ and $\eta_L = 23$ mPa s, representative of the dewetting system studied by Blake and Ruschak (aqueous glycerol solutions on polyester tape) [33].

[3] A <fn0015>better estimate of θ_{crit} and U_{crit} might possibly be obtained by solving Eqs. (3) and (8), however the solution is more complex, less instructive and probably not warranted.

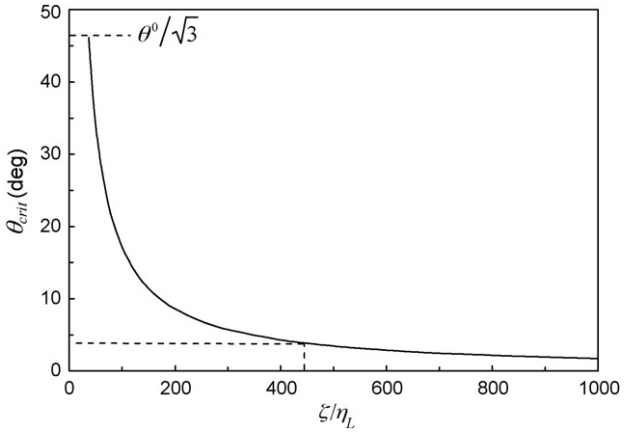

Fig. 8. Critical dynamic contact angle θ_{crit} plotted versus the dimensionless ratio of contact-line friction to viscosity ζ/η_L. Curve calculated using Eq. (17) with values of η_L, γ_L, θ^0 and $\ln l_A^*$ as for Fig. 7. The horizontal dashed line indicates the predicted value in the experiment of Blake and Ruschak [33].

If these arguments are correct, Eqs. (17) and (18) can be used to estimate θ_{crit} and U_{crit} directly. Figs. 8 and 9 illustrate the results of such calculations using the same values of η_L, γ_L, θ^0 and $\ln l_A^*$ as for Fig. 7 and increasing values of ζ expressed as multiples of η_L up to 1000. Experiment suggests that for aqueous systems for which θ_D is a very steep function of U at low speeds, $\zeta \gg \eta_L$ and can be of order $10^2 - 10^3 \eta_L$ [25]. We therefore expect θ_{crit} to be small. For the silicone oils on fluorinated surfaces frequently used in investigations of these phenomena, the value of ζ/η_L is probably much lower of about 40 [15]; therefore, θ_{crit} should be correspondingly greater.

Fig. 8 shows θ_{crit} plotted versus the dimensionless ratio ζ/η_L. The solid curve indicates the range over which a dynamic balance is required. As expected, θ_{crit} will tend to be large when hydrodynamic dissipation dominates and small for systems where contact-line friction is the more important phenomenon. Fig. 9 shows the corresponding values of U_{crit}. Also marked on this chart is the value of U_{crit} = 0.55 cm/s obtained by Blake and Ruschak. This corresponds to $\zeta/\eta_L \sim 440$, which translates to $\theta_{crit} \sim 4^\circ$ (see Fig. 8). Based on this result, it is not surprising that they concluded that the receding angle was essentially zero. de Gennes's $\theta^0/\sqrt{3}$ criterion gives 46°, whereas the value obtained from the maximum in the combined theory (Fig. 5) is 21°.For low contact-line friction silicone

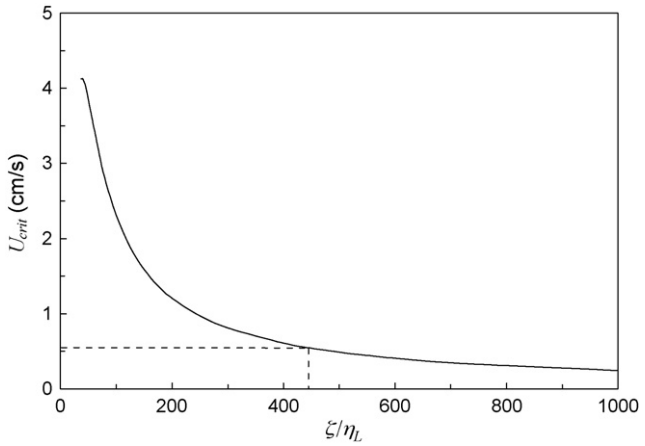

Fig. 9. Critical dewetting velocity U_{crit} plotted versus the dimensionless ratio of contact-line friction to viscosity ζ/η_L. Curve calculated using Eq. (18) with values of η_L, γ_L, θ^0 and $\ln l_A^*$ as for Fig. 7. The horizontal dashed line indicates the value found by Blake and Ruschak [33].

oils on fluoropolymer coated surfaces with $\theta^0 \sim 54^\circ$, Rio et al. [36] found θ_{crit} in the range 33–41°. From an analysis of the data in their Fig. 3a, de Gennes's prediction would be 31°, the combined model would give 26° and our new approach 38°. This is encouraging. However, even if the simple analysis offered here does not provide a complete solution to the problem of predicting θ_{crit}, it should not be taken to mean that the potential influence of contact-line dissipation might be ignored. Better estimates can probably be obtained with more realistic models, such as the Voinov–Cox approach combined with a variable local angle based on contact-line friction or the integrated hydrodynamic model of Shikhmurzaev.

4. Conclusions

We have shown how contact-line friction may play an important role in determining the dynamics of dewetting. This prediction is fully consistent with existing experimental evidence. The arguments presented here also show that the geometry of the system has a strong influence on the mechanism selected. Dewetting initiated by rupture of a continuous film, with the concomitant formation of a rim, differs from that of a film draining under gravity, irrespective of the formation of a serrated contact line. Our new analysis suggests that for a given system, the dynamic contact angles seen in the two cases are also likely to be different. For the growth of a circular hole following rupture of a film previously applied to a partially wetted surface, the angle will be the outcome of hydrodynamic dissipation and contact-line friction operating in parallel at the outer and inner edges of the expanding rim, respectively. For the drainage of a film from a partially wetted surface, the angle may be determined by a dynamic balance between these two dissipation channels that avoids an inflection in the liquid–vapour interface near the receding contact line.

Thus, one model of dewetting does not fit all cases, a conclusion that could be tested readily by new experiments, using the same liquid–solid systems in both geometries. The study should include the measurement of θ_D as a function of U as well as the determination of rim speeds and the maximum dewetting speeds under drainage. To the best of our knowledge, this has never been done in a systematic way, and not at all for systems with a high ratio of contact-line friction to viscosity. The results would enable some of the ideas explored here to be tested rigorously and should lead to better theories and a greater understanding of an important phenomenon.

A large equilibrium contact angle will always favour dewetting, since it will both reduce the contact-line friction (Eq. (12)) and increase the driving force. Nevertheless, even if we factor this overriding influence into the arguments set out above, we can see that the equilibrium wettability may still act in rather complex ways to determine the dynamics of dewetting and the precise onset of liquid entrainment [2,8–10].

Acknowledgements

The authors thank the partial financial support of the Fonds National pour la Recherche Scientifique and the Région Wallonne.

References

[1] C. Redon, F. Brochard-Wyart, F. Rondelez, Dynamics of dewetting, Phys. Rev. Lett. 66 (1991) 715–718.
[2] K. Jacobs, R. Seemann, G. Schatz, S. Herminghaus, Growth of holes in liquid films with partial slippage, Langmuir 14 (1998) 4961–4963.
[3] J. Koplik, J.R. Banavar, Molecular simulations of dewetting, Phys. Rev. Lett. 84 (2000) 4401–4404.
[4] E. Bertrand, T.D. Blake, V. Ledauphin, G. Ogonowski, J. De Coninck, D. Fornasiero, J. Ralston, Dynamics of dewetting at the nanoscale using molecular dynamics, Langmuir 23 (2007) 3774–3785.

[5] P.G. de Gennes, Deposition of langmuir–blodgett layers, Colloid Polym. Sci. 264 (1986) 463–465.
[6] F. Brochard-Wyart, P.G. de Gennes, Dynamics of partial wetting, Adv. Colloid Interface Sci. 39 (1992) 1–11.
[7] P.G. de Gennes, F. Brochard, D. Quéré, Capillarity and Wetting Phenomena: Drops, Bubbles, Pearls and Waves, Springer, New York, 2004, p. 153.
[8] R. Fetzer, K. Jacobs, A. Münch, B. Wagner, T.P. Witelski, New slip regimes and the shape of dewetting thin liquid films, Phys. Rev. Lett. 95 (2005) 127801-1–127801-4.
[9] O. Bäumchen, K. Jacobs, Slip effects in polymer thin films, J. Phys. Condens. Matter 22 (2010) 033102-1–033102-21.
[10] T. Vilmin, E. Raphaël, Dewetting of thin viscoelastic polymer films on slippery substrates, Europhys. Lett. 72 (2005) 781–785.
[11] C. Huh, L.E. Scriven, Hydrodynamic model of steady movement of a solid/liquid/fluid contact line, J. Colloid Interface Sci. 35 (1971) 85–101.
[12] O.V. Voinov, Hydrodynamics of wetting, Fluid Dyn. 11 (1976) 714–721.
[13] R.G. Cox, The dynamics of the spreading of liquids on a solid surface. Part 1. Viscous flow, J. Fluid Mech. 168 (1986) 169–194.
[14] Y.D. Shikhmurzaev, Moving contact lines in liquid/liquid/solid systems, J. Fluid Mech. 334 (1997) 211–249.
[15] T.D. Blake, The physics of moving wetting lines, J. Colloid Interface Sci. 299 (2006) 1–13.
[16] Y.D. Shikhmurzaev, The moving contact line on a smooth solid surface, J. Multiphase Flow 19 (1993) 589–610.
[17] T.D. Blake, J.M. Haynes, Kinetics of liquid/liquid displacement, J. Colloid Interface Sci. 30 (1969) 421–423.
[18] T.D. Blake, Dynamic contact angles and wetting kinetics, in: J.C. Berg (Ed.), Wettability, Marcel Dekker, New York, 1993, pp. 251–309.
[19] T.D. Blake, Current problems in the theory of froth flotation, Ver. Deut. Ing. Berlin 182 (1973) 117–121.
[20] R. Fetzer, J. Ralston, Dynamic dewetting regimes explored, J. Phys. Chem. C. 113 (2009) 8888–8894.
[21] M.J. de Ruijter, T.D. Blake, J. De Coninck, Dynamic wetting studied by molecular modeling simulations of droplet spreading, Langmuir 15 (1999) 7836–7847.
[22] J. De Coninck, T.D. Blake, Wetting and molecular-dynamics simulations of simple liquids, Annu. Rev. Mater. Res. 38 (2008) 15.1–15.22.
[23] E. Bertrand, T.D. Blake, J. De Coninck, Influence of solid–liquid interactions on dynamic wetting: a molecular dynamics study, J. Phys. Condens. Matter 21 (2009) 46124-1–46124-14.
[24] T.D. Blake, J. De Coninck, The influence of solid–liquid interactions on dynamic wetting, Adv. Colloid Interface Sci. 96 (2002) 21–36.
[25] M.J. Vega, C. Gouttière, D. Seveno, T.D. Blake, M. Voué, J. De Coninck, Experimental investigation of the link between static and dynamic wetting by forced wetting of a nylon filament, Langmuir 23 (2007) 10628–10634.
[26] S. Ray, R. Sedev, C. Priest, J. Ralston, Influence of the work of adhesion on the dynamic wetting of chemically heterogeneous surfaces, Langmuir 24 (2008) 13007–13012.
[27] J.G. Petrov, B.P. Radoev, Steady motion of the three phase contact line in model Langmuir–Blodgett systems, Colloid Polym. Sci. 259 (1981) 753–760.
[28] P.G. Petrov, J.G. Petrov, A combined molecular-hydrodynamic approach to wetting kinetics, Langmuir 8 (1992) 1762–1767.
[29] M.J. de Ruijter, J. De Coninck, G. Oshanin, Droplet spreading: partial wetting regime revisited, Langmuir 15 (1999) 2209–2216.
[30] E. Bertrand, Dynamics of liquids at solid surfaces: wetting, dewetting and slip, Ph.D. Thesis, University of Mons, 2009.
[31] L.D. Landau, B.V. Levitch, Dragging of a liquid by a moving plate, Acta Physico-Chim. USSR 17 (1942) 42–54.
[32] B.V. Derjaguin, S.M. Levi, Film Coating Theory, Focal Press, London, 1964, p. 140.
[33] T.D. Blake, K.J. Ruschak, A maximum speed of wetting, Nature 282 (1979) 489–491.
[34] J.H. Snoeijer, G. Delon, M. Fermegier, B. Andreotti, Avoided critical behaviour in dynamically forced wetting, Phys. Rev. Lett. 96 (2006) 174504-1–174504-4.
[35] T. Podgorski, J.M. Flesselles, L. Limat, Corners, Cusps, and pearls in running drops, Phys. Rev. Lett. 87 (2001) 036102-1–036102-4.
[36] E. Rio, A. Daerr, B. Andreotti, L. Limat, Boundary conditions in the 'vicinity of a dynamic contact line: experimental investigation of viscous drops sliding down an inclined plane, Phys. Rev. Lett. 94 (2005) 024503-1–024503-4.
[37] N. Le Grand, A. Daerr, L. Limat, Shape and motion of drops sliding down an inclined plane, J. Fluid Mech. 541 (2005) 293–315.
[38] T.D. Blake, K.J. Ruschak, Wetting: static and dynamic contact lines, in: P.M. Schweizer, S.F. Kistler (Eds.), Liquid Film Coating, Chapman & Hall, London, 1997, pp. 63–97.
[39] C.L. Bower, E.A. Simister, E. Bonnist, K. Paul, N. Pightling, T.D. Blake, Continuous coating of discrete areas of a flexible web, AIChE J. 53 (2007) 1644–1657.
[40] J.G. Petrov, R.V. Sedev, On the existence of a maximum speed of wetting, Colloids Surf. 13 (1985) 313–322.
[41] P.G. Petrov, Dynamics of deposition of Langmuir–Blodgett multilayers, J. Chem. Soc., Faraday Trans. 93 (1997) 295–302.
[42] J. Eggers, Hydrodynamic theory of forced dewetting, Phys. Rev. Lett. 93 (2004) 094502-1–094502-4.
[43] T.D. Blake, The contact angle and two-phase flow, Ph.D. Thesis, University of Bristol, 1968.
[44] D. Quéré, E. Archer, The trail of the drops, Europhys. Lett. 24 (1993) 761–766.
[45] R.V. Sedev, J.G. Petrov, Influence of geometry of the three-phase system on the maximum speed of wetting, Colloids Surf. 34 (1988/1989) 197–201.
[46] J.G. Petrov, R. Sedev, P.G. Petrov, Effect of geometry on steady wetting kinetics and critical velocity of film entrainment, Adv. Colloid Interface Sci. 38 (1992) 229–269.
[47] J.H. Snoeijer, N. Le Grand-Piteira, L. Limat, H.A. Stone, J. Eggers, Cornered drops and rivulets, Phys. Fluids 19 (2007) 042104-1–042104-10.